CHAPTER 3

METABOLIC ALTERATIONS IN ONCOGENE-INDUCED SENESCENCE

Manuscript in preparation

METABOLIC ALTERATIONS IN ONCOGENE-INDUCED SENESCENCE

Joanna Kaplon[1], Liang Zheng[2], Vitaly A. Selivanov[3,4], Marta Cascante[3,4], Tomer Shlomi[5], Eyal Gottlieb[2] and Daniel S. Peeper[1]

[1]Division of Molecular Oncology, The Netherlands Cancer Institute, Plesmanlaan 121, 1066 CX Amsterdam, The Netherlands. [2]Cancer Research UK, Beatson Institute for Cancer Research, Switchback Road, Glasgow G61 1BD, Scotland, UK. [3]Department of Biochemistry and Molecular Biology, Faculty of Biology, Universitat de Barcelona, Av Diagonal 643, 08028 Barcelona, Spain. [4]Institute of Biomedicine of Universitat de Barcelona (IBUB) and CSIC-Associated Unit, Spain. [5]Computer Science Department, Technion, Israel Institute of Technology, Haifa, 32000, Israel.

SUMMARY

Oncogene-induced senescence (OIS) represents a powerful pathophysiological mechanism suppressing cancer. While deregulation of metabolism is an important feature of cancer, little is known about the role of cellular metabolism in OIS. Here, we performed an unbiased analysis of the central carbon metabolism in cells undergoing OIS and found that senescence is associated with a distinct metabolic profile. OIS cells show an increased rate of pyruvate oxidation in mitochondria, less utilization of glutamine and an increased rate of fatty acid secretion. These metabolic changes directly oppose those observed in cancer, indicating that the antitumor function of OIS is manifested also on the level of metabolic regulation.

INTRODUCTION

Multicellular organisms have the capacity to renew, repair and regenerate tissues, allowing for the maintenance of proper tissue and organ functions. A downside of the ability to self-renew is the risk that this process goes wrong and culminates in uncontrolled cell proliferation, with cancer as a prime example. Different mechanisms have developed to prevent oncogenic transformation. Some cell types undergo various cell death programs such as apoptosis[1] or autophagy[2]. Others follow an alternative tactic: they stop proliferating and enter a phase called senescence. Indeed, antitumor function of oncogene-induced senescence (OIS) has been clearly demonstrated *in vivo* both in mouse models and human samples[3]. Because of the substantial role for OIS in the prevention of cancer, great effort is being made to disclose that process. However, despite enormous progress, we are only beginning to reveal the molecular mechanism of OIS.

Numerous studies have shown that deregulation of metabolism is closely linked to the proliferative potential of cells[4-8]. To support a high rate of proliferation, cancer cells commonly shift their metabolism towards biosynthesis, thereby providing the building

blocks necessary for tumor expansion. Metabolic pathways are therefore rewired such that anabolic processes are executed in parallel to programs generating energy production sufficient to sustain cell growth and survival[9].

In spite of the wide belief that senescent cells remain metabolically active[10], few investigators have studied metabolic regulation in senescence in detail. Interestingly, several of the pathways regulating metabolism in tumor cells are linked to senescence. For example, p53, a tumor suppressor contributing to some types of OIS, modulates glucose utilization and mitochondrial respiration. p53 reduces glycolysis by induction of the expression of TIGAR, an enzyme downregulating levels of the glycolytic activator fructose-2,6-bisphosphate (F-2,6-BP)[11] and a simultaneous inhibition of the expression of glucose transporters GLUT 1 and GLUT4[12] and glycolytic enzyme phosphoglycerate mutase (PGM)[13]. Consequently, activation of glycolysis by overexpression of PGM abrogates p53-dependent senescence[13]. At the same time, p53 promotes mitochondrial respiration by transcriptional activation of subunit I of cytochrome c oxidase[14] and activation of expression of synthesis of cytochrome c oxidase 2 (SCO2)[15]. Along these lines, recently a connection has been made between tricarboxylic acid cycle (TCA) associated malic enzymes (MEs) and p53-dependent senescence[16]. While p53 accumulation repressed the expression of ME1 and ME2, and therefore cell metabolism and proliferation, depletion of ME1 and ME2 reciprocally activated p53 in a forward feeding manner, leading to a strong induction of senescence. Also, regulation of nucleotide synthesis has been linked to OIS[17]: ribonucleotide reductase subunit M2 (RRM2), a rate-limiting protein in dNTP synthesis, is downregulated in senescence, resulting in suppression of nucleotide metabolism and DNA synthesis. A decrease in nucleotide pools is crucial for OIS as either addition of exogenous nucleosides or restoration of RRM2 abrogates senescence response. Moreover, we have demonstrated that OIS is associated with increased TCA cycle activity. This is mediated by the activation of the mitochondrial gatekeeper pyruvate dehydrogenase (PDH) as an enzyme linking glycolysis and oxidative phosphorylation[18]. While simultaneous deregulation of PDH-inhibitory kinase PDK1 and its activating phosphatase PDP2 switches on PDH and the OIS program, restoration of the levels of these enzymes inactivates PDH and leads to OIS escape. Interestingly, therapy-induced senescence (TIS) is also associated with enhanced glucose utilization in the TCA cycle[19]. Similarly, analysis of changes in protein expression in OIS revealed an upregulation of proteins involved in oxidative phosphorylation and a downregulation of proteins involved in glycolysis, further supporting an important role for oxidative metabolism in the senescence program[20].

This together demonstrates that senescence and metabolism are tightly intertwined. However, in spite of these observations, a comprehensive study of cellular metabolism in OIS has been lacking. Here, we used mass balance analysis and metabolic flux profiling to screen in an unbiased fashion for metabolic changes accompanying OIS.

RESULTS

We compared the metabolism of human diploid fibroblasts (HDF) undergoing OIS to that of cycling cells. To evoke OIS, we used oncogenic $BRAF^{V600E}$, a common and strong inducer of OIS *in vitro* and *in vivo*[18,21-24]. With the use of liquid-chromatography mass spectrometry (LC-MS), we have quantified the metabolic exchange rate of key metabolites (glucose, lactate, glutamine, glutamate, pyruvate and alanine) as well as their intracellular concentrations. We utilized two independent models, namely mass-balance and isotopomer dynamics, to calculate and predict intracellular metabolic fluxes.

Mass balance analysis predicts differential glutamine, pyruvate and fatty acid metabolism in OIS and cycling cells

In order to understand the potential metabolic alterations taking place during OIS, we delineated a mass-balance model utilizing the measured exchange rates of glucose, lactate, glutamine and glutamate, as well as that of pyruvate itself and alanine, a direct transamination product of pyruvate. Furthermore, the biosynthetic constraint of proliferating cells was translated to the required rate of production and utilization of amino acids, fatty acids and nucleotides. The doubling time of the cycling cells studied is 24 hours and the measured protein concentration is 165 $\mu g/10^6$ cells. Based on these observations, and (for simplicity's sake) assuming an equal distribution of amino acids in proteins and an average molecular weight of an amino acid of 146 g/mol, we calculated the required rate for protein synthesis of key amino acids (which are either absent from the medium or directly derived from reactions in the model (alanine, aspartate, asparagine, glutamine and glutamate)), to be 2.3 nmol/(10^6 cells/hour). Assuming that the dry mass of cells consists of approximately 60% proteins, 20% lipids and 15% nucleotides[25] and that the molecular weight of palmitate (as a readout for fatty acids) is 256 g/mol and the average molecular weight of nucleotide (monophosphate) is 340 g/mol, the rates of lipid (as palmitate equivalents) and nucleotide accumulation as biomass in proliferating cells were calculated to be 8.8 nmol/(10^6 cells/hour) and 5.0 nmol/(10^6 cells/hour), respectively. Finally, oxygen consumption rate (OCR) was measured and utilized in this model to account for the oxidation rate of NADH (2 mol NADH per mol O_2) produced in all the studied reactions.

We fitted these measured and estimated fluxes into a central carbon metabolism model depicted in Figure 1, and calculated the best possible way to balance those metabolic rates in one consistent model. Due to multiple ways to transfer electrons between mitochondrial and cytosolic NAD(P)H/$FADH_2$, a single pool representing all of the latter metabolites was assumed. The production (reduction) rate of these reducing equivalents was fitted into all the known reactions in the model (glycolysis, pentose phosphate pathway, malic enzyme and the TCA cycle).

The mass balance analysis made several predictions:
(1) Glutamine utilization in cycling cells is sufficient to account for the required amino acids, which are either derived directly from glutamine (glutamine and glutamate) or from the TCA cycle (aspartate and asparagine), as well as for pyrimidine biosynthesis. On the other hand, OIS cells produce and secrete more glutamate from glucose (no net glutaminolysis) and hence require an active pyruvate carboxylase (PC) to support anaplerosis. Indeed, when cells were incubated for 24 hours in uniformly labeled [U-$^{13}C_6$]-glucose, and heavy [^{13}C] isotopes were traced in different metabolites, it was evident that more glutamate was derived from glucose in OIS cells as compared to cycling cells and that citrate was labeled with 3 and 5 [^{13}C] carbons, indicative of more pyruvate carboxylase activity in OIS cells (Figure 1).
(2) The mass balance analysis computed a large increase in the rate of pyruvate oxidation by PDH in the mitochondria (Figure 1). This calculation was supported by the fact that OIS cells consumed a similar amount of glucose as cycling cells, but showed less alanine or pyruvate secretion (Figure 1), which was not balanced by an increase in biomass production (as OIS cells do not proliferate). It was also consistent with an increase in OCR in OIS cells, suggesting an increased rate of oxidative phosphorylation. In addition to that, measurements of decreased glutamine uptake and increased glutamate secretion in OIS cells supported the prediction of increased oxidation of pyruvate in these cells (Figure 1).
(3) Although an increase in OCR during OIS was measured, this was insufficient to account for a complete oxidation of the excess pyruvate in the mitochondria. Therefore, it was predicted that the citrate/malate shuttle would remove excess acetyl-CoA (AcCoA) to the cytosol to be used for fatty acids biosynthesis (calculated in palmitate equivalents). Interestingly, the mass balance predicted that the rate of *de novo* palmitate synthesis in cycling cells is insufficient to support the minimum lipid biosynthesis required to sustain the measured proliferation rate and hence cycling cells will require a net uptake of exogenous fatty acids. On the other hand, the higher rate of palmitate production in OIS would require fatty acid secretion. These predictions were experimentally confirmed by LC-MS analyses of extracellular palmitate, oleate and stearate (Figure 1).
To compute the difference in PDH flux between the OIS and cycling cells, while accounting for experimental error in the measurement of metabolite uptake and secretion rates, we assumed a Gaussian noise model per each uptake and secretion measurement (considering the experimental mean and standard deviation in uptake and secretion flux measurements). The standard deviation and confidence interval of PDH flux were calculated based on a linear combination of normal distributions. The expected difference in PDH fluxes (presented as nmol/(10^6 cells x hour) between OIS and cycling cells are:

OIS: PDH = 307.570	std = 79.937	95% CI = [176.085, 439.055]
Cycling: PDH = 63.050	std = 43.106	95% CI = [-7.853, 133.953]
PDH difference = 244.520	std = 90.819	95% CI = [95.136, 393.904]

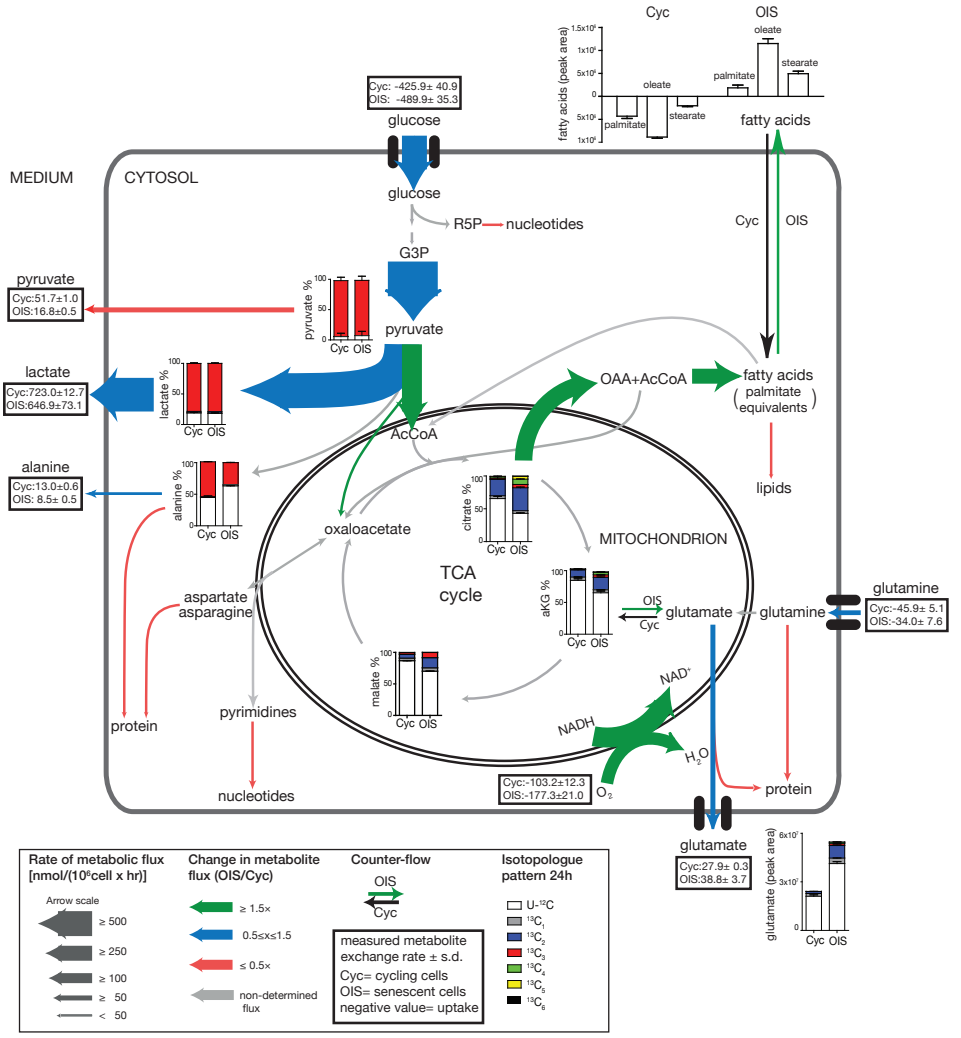

Figure 1. OIS is accompanied by changes in metabolism of glutamine, pyruvate and fatty acids

Metabolic alterations in OIS versus cycling cells were studied using the mass-balance model. Measured metabolic fluxes used for balancing the delineated metabolic network are indicated in solid boxes. The biosynthetic constraint of proliferating cells was translated to the required rate of production and utilization of amino acids, fatty acids and nucleotides. Based on these rates, the remainder of the reactions was fitted to balance the rates of metabolite production with their consumption and/or secretion. Also the rates of reactions that produce reducing equivalents (NAD(P)H and $FADH_2$), (i.e., glycolysis, pentose phosphate pathway, malic enzyme and TCA cycle) were balanced with those that oxidize them (oxygen consumption, lactate dehydrogenase and fatty acid biosynthesis). The calculated reaction rates are presented as colored arrows where the thickness of the arrows represents the rate of reaction and the color represents the ratio between OIS to cycling (cyc) cells. All reactions are calculated as nmol/(10^6 cells x hour). Additional experimental data that provide important support for the predictions made by this model are presented as bar graphs. These represent the levels of metabolites (intracellular and extracellular) and isotopomers derived from [U-$^{13}C_6$]-glucose after 24 hours incubation. AcCoA - acetyl-CoA; G3P - glyceraldehyde 3-phosphate; OAA - oxaloacetate; aKG - alpha-ketoglutarate; R5P - ribose-5-phosphate; TCA cycle - tricarboxylic acid cycle.

Isotopomer flux analysis confirms an increase in the flux of pyruvate into the TCA cycle

To validate the predicted increased rate of pyruvate oxidation in the mitochondria during OIS, we employed a ^{13}C-tracer-based metabolic flux analysis to study the fate of glucose in these cells. For labeling experiments, cycling and OIS cells were incubated with medium supplemented with uniformly labeled [U-$^{13}C_6$]-glucose and at the time points between 15 minutes and 24 hours the distribution of glucose-derived isotopomers of key metabolites was quantified (Supplementary Tables 1 and 2). These metabolic fluxes, which were not measured directly, were determined based on fitting the measured distribution of [^{13}C] isotopic isomers (isotopomers) of intracellular and secreted metabolites (Supplementary Tables 1 and 2) by the isotopomer dynamics method[26]. This method is based on the simulation of dynamics of isotopomer distributions and does not require reaching isotopic steady state. Application of this method was justified by the measured slow dynamics of metabolite labeling. The model consists of a system of ordinary differential equations describing the time course of concentrations of all the measured isotopomers. The algorithms for data fitting and determination of confidence intervals for metabolic fluxes are described in reference 27. Examples of fitting such data for cycling and OIS cells are shown in Figure 2. The fluxes are determined from fitting the entire set of the experimental data shown in Supplementary Table 1. Since the fraction of secreted lactate, pyruvate and alanine with respect to consumed glucose is less in OIS compared to cycling cells, the former directs much more pyruvate into citrate, a combined reaction of PDH and citrate synthase. This is clearly demonstrated by the fact that OIS cells have a higher concentration of citrate, which is labeled faster than in cycling cells (Supplementary Table 1). Table 1 shows the 95% confidence intervals (CI) for the metabolic fluxes. The intervals calculated for cycling and OIS cells are based on fitting the measured fluxes and distribution of isotopomers using the $\chi 2$ (sum of normalized squared deviation between measured and computed data) criterion as described in reference 27. Oxygen consumption (VO_2) is calculated as the combined metabolic rates of PDH + (aKG → Mal) + (Cit → aKG)/2 + MDH/2. This calculation takes into account that conversion of 1 mol of pyruvate into AcCoA results in a reduction of 2 mol of NAD^+ into NADH (one by GAPDH in the cytosol and another by PDH); further conversion in combined reactions (aKG → Mal) result in 1 mol NADH and 1 mol reduced FAD; the reactions (Cit → aKG) and MDH result in reduction of 1 mol NAD^+ each. Oxidation of 2 mol NADH or $FADH_2$ results in a reduction of one mol of oxygen. Thus, as predicted by mass balance analysis, the isotopomer flux analysis identified a sharp increase in the flux into the TCA cycle via PDH in OIS cells when compared to cycling cells.

DISCUSSION

In recent years, the mechanism of cellular metabolism, and its deregulation during oncogenic transformation, has been receiving more attention. The development of sensitive analytic

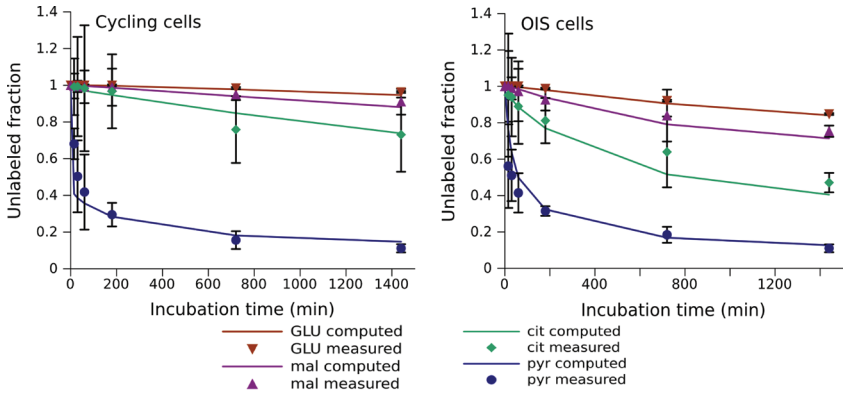

Figure 2. A comparison between the experimental measurements to computational fitting of the rate of glucose-derived ^{13}C incorporation into each indicated metabolite

Time course of unlabeled fractions of metabolites produced by cycling and OIS cells incubated with [U-$^{13}C_6$]-glucose is shown. Measured values with their standard deviations are indicated by symbols and the respective calculated values (best fit) are connected with lines. GLU - glutamate; mal - malate; cit - citrate; pyr - pyruvate.

Table 1.

	cycling		OIS	
	min	**max**	**min**	**max**
Gluc in	411.43	411.43	484.69	484.69
Lac&Pyr out	811.10	812.01	782.33	812.95
ALA out	3.78	4.29	1.19	1.44
Pyr → AcCoA (PDH)	3.35	4.15	140.34	159.41
Pyr → OAA (PC)	0	0	0.07	8.25
aKG → Mal	49.16	54.19	14.59	18.97
aKG → OOA (MDH)	49.16	54.19	14.59	18.97
GLU out	26.18	27.49	21.62	27.28
GLN in	47.14	47.14	24.28	30.55
VO_2	98.28	108.06	169.64	189.98

95% confidence intervals of the indicated reaction rates [nmol/(10^6 cells x hour)]
Gluc - glucose; Lac - lactate; Pyr - pyruvate; AcCoA- Acetyl-CoA; OAA - oxaloacetate; aKG - alpha-ketoglutarate; Mal - malate; GLU - glutamate; GLN - glutamine; PDH- pyruvate dehydrogenase; PC - pyruvate carboxylase; MDH - malate dehydrogenase.

tools to monitor metabolism in living cells has deepened our understanding of metabolic regulation. However, in spite of the widely recognized importance of OIS, and particularly abrogation thereof, for oncogenic transformation, little is known about the regulation and role of cellular metabolism in this context. For example, it is unclear how metabolic fluxes change when cells undergo OIS, and whether they are functionally connected to the execution of the senescence program.

Here, we report an unbiased and comprehensive analysis of the central carbon metabolism in cells undergoing OIS. Our study reveals that OIS cells display several metabolic alterations when compared to cycling cells. Both mass balance and isotopomer flux analyses show that entry into OIS is accompanied by an increase in pyruvate flux into the TCA cycle. Specifically, the rate of conversion of pyruvate to citrate, a combined reaction of PDH and citrate synthase, is highly increased during OIS. Notably, we have previously identified PDH to be an important modulator of OIS[18]. We have shown that PDH is activated in OIS due to the deregulation of expression levels of PDH regulatory enzymes: PDK1 and PDP2. Also, we have demonstrated that this process is not merely an epiphenomenon accompanying OIS as enforced normalization of the PDK1 or PDP2 levels resulted in an efficient abrogation of OIS. The fact that we found PDH to be activated in OIS not only confirms our previous observations, but also illustrates the versatility of metabolic modeling approaches to identify novel candidate pathways central for senescence program.

Another prediction that arose from our metabolic profiling is that OIS cells have altered their glutamine metabolism when compared to cycling cells. Interestingly, pharmacological inhibition of glutaminase (GLS), the first enzyme involved in glutaminolysis, was shown to induce premature senescence in endothelial cells[28]. Notably, activity of GLS isozymes has been correlated to growth rates and malignancy in tumors. Along these lines, silencing of GLS expression or inhibition of its activity delayed tumor growth[29-31]. As several hallmarks of malignancy depend on the presence of glutamine[32], a downregulation of glutamine utilization in OIS is likely to represent a tumor-suppressive response. Hence, from a therapeutic point of view, it would be interesting to study the regulation of glutamine in senescence in more detail.

Next to the higher rate of pyruvate oxidation and alteration of glutamine metabolism in OIS, our study predicts that OIS is accompanied by an alteration in fatty acid metabolism. Notably, a few studies have previously linked senescence to changes in lipogenesis. For example, senescence was demonstrated to associate with reduced formation of phospholipids as well as biosynthesis and desaturation of fatty acid[33]. Along these lines, senescent cells showed an increased ratio of glycerophosphocholine (GPC) to phosphocholine (PC), both important in phospholipid metabolism[34]. Interestingly, the observed changes in the choline metabolism counteract the well-known changes in choline metabolism of tumor cells, which show a "GPC to PC switch"[35-37]. Moreover, OIS cells were shown to have an increased steady-state level of certain free fatty acids[38]. Higher fatty acid levels do not reflect an increase in *de novo* synthesis of fatty acids, as the rates of lipid synthesis are reduced in OIS cells, but correlate with an increased rate of fatty acid oxidation. Nevertheless, inhibiting the fatty acid oxidation did not prevent a senescence-associated cell cycle arrest[38], arguing against a causal role of that process in senescence. These observations, together with an increasing role of lipid metabolism in tumorigenesis[39,40], suggest that modulating this metabolic

pathway in senescence is a mechanism to prevent malignant transformation. Studying the nature of that regulation will be of great interest as it might reveal attractive therapeutic metabolic cancer targets.

MATERIALS AND METHODS

Cell culture, viral transduction, and senescence induction

The human diploid fibroblast (HDF) cell line TIG3 expressing the ectopic receptor, hTERT and sh-p16^{INK4A} was maintained in DMEM, supplemented with 9% fetal bovine serum (PAA), 2 mM glutamine, 100 units/ml penicillin and 0.1 mg/ml streptomycin (GIBCO). Retroviral infections were performed using Phoenix cells as producers of viral supernatants. For senescence induction, HDFs were infected with BRAF^{V600E}-encoding or control virus and pharmacologically selected with blasticidin. Cells were analyzed at the day 9 after introduction of BRAF^{V600E}, the day that senescence is fully established.

Plasmids

pMSCV-blast-BRAF^{V600E} and pMSCV-blast were previously described[24].

Measurement of metabolites by LC-MS

2×10^6 HDF were plated onto 10-cm dishes and cultured in standard medium for 24 hours. For ^{13}C-flux analysis, the medium was replaced with 4.5 mM [U-^{13}C]-glucose (Cambridge Isotope, UK). After incubation for the indicated time, cells and media were collected. For extracellular metabolite analysis, 200 µL of growth media from cell culture were added to 600 µL of acetonitrile for deproteinization. Samples were vortexed for 10 minutes and centrifuged for 10 minutes at 16000 g at 4 ^{0}C. The supernatant was stored for subsequent LC-MS analysis. For intracellular metabolite analysis, cells were lysed with a solution composed of 50% methanol and 30% acetonitrile in water in dry iced methanol (-80 ^{0}C) and quickly scraped from the plate. The insoluble material was immediately pelleted in a cooled centrifuge (4 ^{0}C) for 10 minutes at 16000 g and the supernatant was collected for subsequent LC-MS analysis. LC-MS analysis was carried out as described in reference 41. MS data was analyzed by LCquan™ (Thermo Scientific, UK) and quantifications of intracellular and extracellular metabolites were performed by the standard-dilution method as describe in reference 42.

REFERENCES

1. Lowe, S. W., Cepero, E. & Evan, G. Intrinsic tumour suppression. *Nature* **432,** 307–315 (2004).
2. Mathew, R., Karantza-Wadsworth, V. & White, E. Role of autophagy in cancer. *Nat Rev Cancer* **7,** 961–967 (2007).
3. Collado, M. & Serrano, M. Senescence in tumours: evidence from mice and humans. *Nat Rev Cancer* **10,** 51–57 (2010).
4. Cantor, J. R. & Sabatini, D. M. Cancer cell metabolism: one hallmark, many faces. *Cancer Discov* **2,** 881–898 (2012).
5. DeBerardinis, R. J., Sayed, N., Ditsworth, D. & Thompson, C. B. Brick by brick: metabolism and tumor cell growth. *Curr Opin Genet Dev* **18,** 54–61 (2008).
6. Tennant, D. A., Durán, R. V. & Gottlieb, E. Targeting metabolic transformation for

cancer therapy. *Nat Rev Cancer* **10,** 267–277 (2010).
7. Vander Heiden, M. G., Cantley, L. C. & Thompson, C. B. Understanding the Warburg effect: the metabolic requirements of cell proliferation. *Science* **324,** 1029–1033 (2009).
8. Wellen, K. E. & Thompson, C. B. Cellular metabolic stress: considering how cells respond to nutrient excess. *Mol Cell* **40,** 323–332 (2010).
9. Lunt, S. Y. & Vander Heiden, M. G. Aerobic glycolysis: meeting the metabolic requirements of cell proliferation. *Annu. Rev. Cell Dev. Biol.* **27,** 441–464 (2011).
10. Campisi, J. Replicative senescence: an old lives' tale? *Cell* **84,** 497–500 (1996).
11. Bensaad, K. *et al.* TIGAR, a p53-inducible regulator of glycolysis and apoptosis. *Cell* **126,** 107–120 (2006).
12. Schwartzenberg-Bar-Yoseph, F., Armoni, M. & Karnieli, E. The tumor suppressor p53 down-regulates glucose transporters GLUT1 and GLUT4 gene expression. *Cancer Res* **64,** 2627–2633 (2004).
13. Kondoh, H. *et al.* Glycolytic enzymes can modulate cellular life span. *Cancer Res* **65,** 177–185 (2005).
14. Okamura, S. *et al.* Identification of seven genes regulated by wild-type p53 in a colon cancer cell line carrying a well-controlled wild-type p53 expression system. *Oncol. Res.* **11,** 281–285 (1999).
15. Matoba, S. *et al.* p53 regulates mitochondrial respiration. *Science* **312,** 1650–1653 (2006).
16. Jiang, P., Du, W., Mancuso, A., Wellen, K. E. & Yang, X. Reciprocal regulation of p53 and malic enzymes modulates metabolism and senescence. *Nature* **493,** 689–693 (2013).
17. Aird, K. M. *et al.* Suppression of nucleotide metabolism underlies the establishment and maintenance of oncogene-induced senescence. *CellReports* **3,** 1252–1265 (2013).
18. Kaplon, J. *et al.* A key role for mitochondrial gatekeeper pyruvate dehydrogenase in oncogene-induced senescence. *Nature* **498,** 109–112 (2013).
19. Dörr, J. R. *et al.* Synthetic lethal metabolic targeting of cellular senescence in cancer therapy. *Nature* **501,** 421–425 (2013).
20. Li, M. *et al.* Oncogene-induced cellular senescence elicits an anti-Warburg effect. *Proteomics* **13,** 2585–2596 (2013).
21. Dankort, D. *et al.* Braf(V600E) cooperates with Pten loss to induce metastatic melanoma. *Nat Genet* **41,** 544–552 (2009).
22. Dhomen, N. *et al.* Oncogenic Braf induces melanocyte senescence and melanoma in mice. *Cancer Cell* **15,** 294–303 (2009).
23. Michaloglou, C. *et al.* BRAFE600-associated senescence-like cell cycle arrest of human naevi. *Nature* **436,** 720–724 (2005).
24. Kuilman, T. *et al.* Oncogene-Induced Senescence Relayed by an Interleukin-Dependent Inflammatory Network. *Cell* **133,** 1019–1031 (2008).
25. Frezza, C. *et al.* Haem oxygenase is synthetically lethal with the tumour suppressor fumarate hydratase. *Nature* **477,** 225–228 (2011).
26. Selivanov, V. A., Marin, S., Lee, P. W. N. & Cascante, M. Software for dynamic analysis of tracer-based metabolomic data: estimation of metabolic fluxes and their statistical analysis. *Bioinformatics* **22,** 2806–2812 (2006).
27. de Mas, I. M. *et al.* Compartmentation of glycogen metabolism revealed from 13C isotopologue distributions. *BMC Syst Biol* **5,** 175 (2011).
28. Unterluggauer, H. *et al.* Premature senescence of human endothelial cells induced by inhibition of glutaminase. *Biogerontology* **9,** 247–259 (2008).
29. Gao, P. *et al.* c-Myc suppression of miR-23a/b enhances mitochondrial glutaminase expression and glutamine metabolism. *Nature* **458,** 762–765 (2009).
30. Lobo, C. *et al.* Inhibition of glutaminase expression by antisense mRNA decreases growth and tumourigenicity of tumour cells. *Biochem J* **348 Pt 2,** 257–261 (2000).
31. Wang, J.-B. *et al.* Targeting mitochondrial glutaminase activity inhibits oncogenic transformation. *Cancer Cell* **18,** 207–219 (2010).
32. Hensley, C. T., Wasti, A. T. & DeBerardinis, R. J. Glutamine and cancer: cell biology, physiology, and clinical opportunities. *J. Clin. Invest.* **123,** 3678–3684 (2013).
33. Maeda, M., Scaglia, N. & Igal, R. A. Regulation of fatty acid synthesis and Delta9-desaturation in senescence of human fibroblasts. *Life Sci.* **84,** 119–124 (2009).
34. Gey, C. & Seeger, K. Metabolic changes during cellular senescence investigated by proton NMR-spectroscopy. *Mechanisms*

of Ageing and Development **134,** 130–138 (2013).
35. Aboagye, E. O. & Bhujwalla, Z. M. Malignant transformation alters membrane choline phospholipid metabolism of human mammary epithelial cells. *Cancer Res* **59,** 80–84 (1999).
36. Glunde, K., Bhujwalla, Z. M. & Ronen, S. M. Choline metabolism in malignant transformation. *Nat Rev Cancer* **11,** 835–848 (2011).
37. Iorio, E. *et al.* Alterations of choline phospholipid metabolism in ovarian tumor progression. *Cancer Res* **65,** 9369–9376 (2005).
38. Quijano, C. *et al.* Oncogene-induced senescence results in marked metabolic and bioenergetic alterations. *cc* **11,** 1383–1392 (2012).
39. Santos, C. R. & Schulze, A. Lipid metabolism in cancer. *FEBS J* **279,** 2610–2623 (2012).
40. Wymann, M. P. & Schneiter, R. Lipid signalling in disease. *Nat Rev Mol Cell Biol* **9,** 162–176 (2008).
41. Frezza, C. *et al.* Metabolic profiling of hypoxic cells revealed a catabolic signature required for cell survival. *PLoS ONE* **6,** e24411 (2011).
42. Chaneton, B. *et al.* Serine is a natural ligand and allosteric activator of pyruvate kinase M2. *Nature* (2012). doi:10.1038/nature11540

Supplementary Table 1. Intracellular isotopomer quantities [nmol/10^6cells] at the indicated time point (n=3)

Compounds	Cycling 15min		Cycling 30min		Cycling 60min		Cycling 3 hr		Cycling 12 hr		Cycling 24 hr		OIS 15min		OIS 30min		OIS 60min		OIS 3 hr		OIS 12 hr		OIS 24 hr	
	Mean	*SD(±)*	*Mean*	*SD(±)*	*Mean*	*SD(±)*	*Mean*	*SD(±)*	*Mean*	*SD(±)*	*Mean*	*SD(±)*	*Mean*	*SD(±)*	*Mean*	*SD(±)*	*Mean*	*SD(±)*	*Mean*	*SD(±)*	*Mean*	*SD(±)*	*Mean*	*SD(±)*
Glucose +0	12,43	2,77	8,25	2,80	9,78	2,59	8,29	1,56	7,17	1,28	9,64	2,49	5,92	1,29	8,43	1,03	6,57	1,25	8,11	0,23	8,85	1,48	5,39	0,83
Glucose +1	0,74	0,21	0,51	0,20	0,67	0,19	0,54	0,14	0,45	0,08	0,57	0,17	0,37	0,12	0,60	0,08	0,44	0,11	0,55	0,02	0,57	0,16	0,33	0,06
Glucose +5	5,24	0,30	6,52	2,27	5,89	1,72	7,13	1,44	5,10	1,33	6,29	1,75	6,57	2,24	9,49	2,10	5,83	1,27	8,12	0,54	6,92	2,28	4,55	0,78
Glucose +6	97,78	4,29	120,03	42,95	106,51	29,70	128,50	25,58	92,42	24,68	112,90	31,54	90,65	26,24	169,94	38,83	103,72	24,14	143,14	10,09	122,67	37,68	80,61	12,16
Sum	**116,19**	**6,54**	**135,31**	**48,15**	**122,85**	**34,06**	**144,47**	**28,54**	**105,14**	**27,26**	**129,41**	**35,85**	**103,51**	**29,27**	**188,46**	**41,95**	**116,56**	**26,72**	**159,92**	**10,47**	**139,01**	**41,58**	**90,88**	**13,75**
GA3P +0	1,92	0,13	1,14	0,02	1,20	0,15	1,00	0,08	1,05	0,04	1,01	0,13	2,09	0,08	1,46	0,05	1,56	0,26	1,37	0,19	1,21	0,09	1,30	0,05
GA3P +3	1,68	0,16	1,89	0,18	2,12	0,12	2,48	0,22	3,63	0,25	5,37	0,56	6,46	0,84	4,62	0,33	4,60	0,38	4,67	0,47	4,73	0,59	7,54	0,30
Sum	**3,60**	**0,17**	**3,04**	**0,17**	**3,32**	**0,24**	**3,48**	**0,20**	**4,68**	**0,29**	**6,38**	**0,68**	**8,54**	**0,82**	**6,08**	**0,37**	**6,16**	**0,61**	**6,04**	**0,65**	**5,94**	**0,67**	**8,84**	**0,32**
Pyr +0	0,10	0,01	0,10	0,04	0,08	0,04	0,13	0,03	0,17	0,05	0,28	0,06	0,05	0,02	0,07	0,02	0,05	0,01	0,10	0,01	0,18	0,04	0,07	0,01
Pyr +1									0,01	0,00	0,01	0,00									0,00	0,00		
Pyr +2									0,01	0,00	0,05	0,01									0,01	0,00	0,01	0,00
Pyr +3	0,05	0,01	0,10	0,03	0,11	0,04	0,30	0,07	0,89	0,11	2,17	0,62	0,04	0,01	0,07	0,02	0,08	0,02	0,23	0,03	0,77	0,21	0,58	0,11
Sum	**0,15**	**0,01**	**0,21**	**0,07**	**0,20**	**0,08**	**0,43**	**0,10**	**1,07**	**0,16**	**2,51**	**0,69**	**0,09**	**0,03**	**0,13**	**0,02**	**0,13**	**0,04**	**0,33**	**0,03**	**0,96**	**0,25**	**0,66**	**0,13**
Lac +0	18,26	1,21	24,32	8,91	19,53	6,13	21,48	5,22	21,95	5,56	33,53	9,01	29,21	10,42	43,59	6,46	29,83	10,71	41,41	2,16	38,76	10,83	30,59	4,99
Lac +1	0,55	0,06	0,74	0,31	0,64	0,17	0,69	0,18	0,65	0,21	1,07	0,31	0,80	0,27	1,31	0,17	0,92	0,30	1,28	0,07	1,24	0,27	1,06	0,16
Lac +2	0,16	0,01	0,25	0,04	0,30	0,06	0,66	0,14	1,44	0,40	3,61	0,95	0,21	0,02	0,34	0,05	0,37	0,08	0,93	0,06	2,45	0,56	3,66	0,51
Lac +3	5,81	0,33	9,35	1,39	11,27	2,07	24,19	4,87	54,51	13,30	134,46	33,55	8,59	1,80	12,01	1,07	14,21	3,22	34,86	1,46	101,13	24,96	132,47	21,42
Sum	**24,78**	**1,36**	**34,66**	**10,60**	**31,74**	**8,16**	**47,02**	**10,39**	**78,55**	**18,96**	**172,66**	**43,46**	**38,81**	**12,48**	**57,24**	**7,63**	**45,33**	**14,16**	**78,48**	**1,15**	**143,58**	**36,59**	**167,78**	**26,83**
ALA +0	5,87	0,21	5,42	0,36	5,18	0,40	5,77	0,31	5,25	0,50	5,44	0,26	2,38	0,40	2,61	0,15	2,56	0,21	2,98	0,16	3,39	0,26	3,67	0,16
ALA +1	0,18	0,01	0,16	0,01	0,15	0,01	0,17	0,01	0,16	0,01	0,17	0,01	0,06	0,01	0,07	0,01	0,07	0,00	0,08	0,00	0,10	0,01	0,11	0,01
ALA +2	0,00	0,00	0,00	0,00																	0,00	0,00	0,01	0,00
ALA +3	0,66	0,02	0,73	0,02	0,90	0,07	1,79	0,09	3,93	0,43	6,91	0,30	0,10	0,01	0,12	0,01	0,16	0,00	0,40	0,01	0,88	0,12	2,04	0,13
Sum	**6,71**	**0,24**	**6,31**	**0,39**	**6,24**	**0,48**	**7,73**	**0,38**	**9,35**	**0,95**	**12,53**	**0,56**	**2,54**	**0,41**	**2,80**	**0,16**	**2,78**	**0,21**	**3,45**	**0,16**	**4,38**	**0,39**	**5,82**	**0,29**
Citrate +0	0,76	0,13	1,02	0,30	0,65	0,24	1,03	0,23	1,12	0,29	1,93	0,57	2,15	0,82	2,77	0,67	1,91	0,47	2,52	0,41	2,19	0,72	1,98	0,25
Citrate +1	0,05	0,01	0,09	0,04	0,04	0,02	0,06	0,02	0,08	0,02	0,15	0,04	0,15	0,06	0,17	0,04	0,12	0,03	0,18	0,03	0,17	0,05	0,19	0,02
Citrate +2	0,01	0,00	0,01	0,00	0,01	0,00	0,04	0,01	0,34	0,05	0,64	0,13	0,11	0,03	0,17	0,01	0,24	0,02	0,52	0,09	1,00	0,16	1,60	0,11
Citrate +3									0,02	0,00	0,04	0,01	0,01	0,00	0,01	0,00	0,01	0,00	0,05	0,01	0,12	0,01	0,23	0,02
Citrate +4									0,01	0,00	0,06	0,01							0,04	0,01	0,15	0,02	0,37	0,02
Citrate +5									0,01	0,00	0,02	0,00							0,01	0,00	0,07	0,01	0,19	0,02
Citrate +6																					0,00	0,00	0,03	0,00
Sum	**0,81**	**0,14**	**1,11**	**0,33**	**0,70**	**0,26**	**1,13**	**0,25**	**1,58**	**0,35**	**2,84**	**0,77**	**2,42**	**0,90**	**3,12**	**0,72**	**2,28**	**0,48**	**3,33**	**0,55**	**3,69**	**0,95**	**4,59**	**0,43**
a-KG +0	0,52	0,04	0,69	0,06	0,76	0,10	1,07	0,13	1,75	0,25	2,45	0,17	0,19	0,02	0,24	0,01	0,27	0,03	0,32	0,01	0,42	0,06	0,58	0,03
a-KG +1	0,03	0,00	0,03	0,00	0,04	0,01	0,06	0,01	0,10	0,01	0,14	0,01	0,01	0,00	0,01	0,00	0,01	0,00	0,02	0,00	0,03	0,00	0,04	0,00
a-KG +2									0,11	0,01	0,30	0,02			0,00	0,00	0,01	0,00	0,03	0,00	0,08	0,01	0,17	0,01
a-KG +3									0,01	0,00	0,03	0,00							0,00	0,00	0,01	0,00	0,03	0,00
a-KG +4									0,00	0,00	0,02	0,00							0,00	0,00	0,01	0,00	0,03	0,00
a-KG +5											0,00	0,00									0,00	0,00	0,01	0,00
Sum	**0,55**	**0,04**	**0,72**	**0,06**	**0,80**	**0,11**	**1,13**	**0,14**	**1,97**	**0,28**	**2,94**	**0,20**	**0,20**	**0,02**	**0,26**	**0,01**	**0,29**	**0,04**	**0,37**	**0,01**	**0,56**	**0,08**	**0,87**	**0,05**
Mal +0	0,74	0,05	0,97	0,03	1,25	0,12	1,56	0,17	1,99	0,07	1,96	0,16	0,33	0,07	0,50	0,03	0,53	0,09	0,67	0,04	0,57	0,10	0,60	0,03
Mal +1	0,03	0,00	0,04	0,00	0,05	0,00	0,06	0,01	0,09	0,00	0,10	0,01	0,01	0,00	0,02	0,00	0,02	0,00	0,03	0,00	0,04	0,01	0,05	0,00
Mal +2							0,00	0,00	0,08	0,00	0,14	0,01			0,00	0,00	0,01	0,00	0,04	0,00	0,08	0,01	0,14	0,01
Mal +3	0,00	0,00	0,01	0,00	0,01	0,00	0,02	0,00	0,04	0,00	0,07	0,00			0,00	0,00	0,00	0,00	0,01	0,00	0,04	0,00	0,07	0,01
Sum	**0,77**	**0,06**	**1,02**	**0,03**	**1,31**	**0,12**	**1,64**	**0,17**	**2,19**	**0,07**	**2,26**	**0,18**	**0,34**	**0,07**	**0,52**	**0,03**	**0,57**	**0,10**	**0,76**	**0,05**	**0,72**	**0,13**	**0,85**	**0,04**
GLU +0	113,58	2,86	114,28	1,20	115,31	3,95	115,63	4,62	107,19	3,17	92,59	1,49	58,99	4,13	62,76	1,67	68,90	1,78	63,43	3,37	51,22	1,71	48,89	0,77
GLU +1	6,45	0,17	6,43	0,05	6,51	0,25	6,60	0,32	6,29	0,22	5,65	0,13	3,33	0,21	3,54	0,10	3,71	0,65	4,04	0,23	3,70	0,12	3,88	0,06
GLU +2			0,04	0,01	0,56	0,09	1,79	0,07	7,38	0,32	11,52	0,02	0,76	0,03	1,62	0,02	3,11	0,17	6,90	0,27	10,98	0,27	15,68	0,32
GLU +3									0,42	0,05	0,99	0,03					0,11	0,02	0,66	0,02	1,68	0,05	3,22	0,11
GLU +4									0,20	0,02	0,73	0,03					0,03	0,01	0,40	0,05	1,37	0,05	3,17	0,14
GLU +5											0,01	0,00									0,27	0,02	1,02	0,05
Sum	**120,02**	**3,03**	**120,75**	**1,25**	**122,37**	**4,28**	**124,02**	**5,01**	**121,47**	**3,67**	**111,49**	**1,64**	**63,08**	**4,37**	**67,92**	**1,78**	**75,86**	**2,42**	**75,42**	**3,61**	**69,23**	**2,17**	**75,86**	**1,43**
GLN +0	112,98	3,83	116,39	7,60	108,63	4,29	126,63	6,20	113,85	5,77	122,03	6,86	80,39	16,27	89,49	9,74	79,48	9,42	100,26	3,31	99,31	8,75	96,27	2,01
GLN +1	6,33	0,18	6,56	0,47	6,19	0,27	7,17	0,36	6,47	0,31	6,93	0,39	4,55	0,91	4,99	0,47	4,46	0,57	5,72	0,18	5,63	0,48	5,45	0,12
Sum	**119,31**	**4,00**	**122,95**	**8,07**	**114,81**	**4,55**	**133,80**	**6,56**	**120,32**	**6,08**	**128,96**	**7,25**	**84,94**	**17,17**	**94,47**	**10,21**	**83,94**	**9,99**	**105,98**	**3,49**	**104,94**	**9,23**	**101,72**	**2,13**

Supplementary Table 2. Extracellular isotopomer distribution [%] at the indicated time (n=3)

Compounds	Cycling 15min		Cycling 30min		Cycling 60min		Cycling 3hr		Cycling 12hr		Cycling 24hr		OIS 15min		OIS 30min		OIS 60min		OIS 3hr		OIS 12hr		OIS 24hr	
	Mean	*±SD*	*Mean*	*±SD*	*Mean*	*±SD*	*Mean*	*±SD*	*Mean*	*±SD*	*Mean*	*±SD*	*Mean*	*±SD*	*Mean*	*±SD*	*Mean*	*±SD*	*Mean*	*±SD*	*Mean*	*±SD*	*Mean*	*±SD*
Glucose +0	6,3	0,1	4,9	0,5	5,3	1,2	4,9	0,6	5,9	0,3	5,6	0,6	4,3	0,7	4,3	0,3	5,5	0,7	5,0	0,6	6,1	0,4	5,7	0,3
Glucose +5	4,9	0,0	4,9	0,0	4,9	0,1	4,9	0,0	4,9	0,1	4,9	0,0	5,0	0,0	5,0	0,1	4,9	0,0	4,9	0,0	4,9	0,0	4,9	0,1
Glucose +6	88,8	0,1	90,2	0,5	89,8	1,1	90,2	0,6	89,2	0,4	89,5	0,5	90,7	0,7	90,7	0,3	89,6	0,7	90,0	0,5	89,1	0,4	89,4	0,3
Sum	**100**		**100**		**100**		**100**		**100**		**100**		**100**		**100**		**100**		**100**		**100**		**100**	
Pyr +0	84,1	1,1	70,5	0,4	52,9	0,9	35,6	1,7	21,7	0,7	15,3	0,3	78,0	1,8	67,1	1,4	58,3	1,9	41,3	3,3	23,7	1,2	15,2	0,8
Pyr +1	2,7	0,4	2,3	0,3	1,8	0,1	1,1	0,1	0,7	0,0	0,5	0,0	2,2	0,6	1,9	0,2	1,8	0,4	1,4	0,1	0,8	0,0	0,6	0,0
Pyr +2					1,0	0,1	1,4	0,1	1,9	0,0	2,1	0,2							1,3	0,2	1,9	0,1	2,2	0,0
Pyr +3	13,2	1,1	27,2	0,5	44,4	0,8	61,8	1,9	75,7	0,8	82,1	0,2	19,7	1,2	31,0	1,2	39,9	2,3	56,0	3,1	73,6	1,1	82,0	0,8
Sum	**100**		**100**		**100**		**100**		**100**		**100**		**100**		**100**		**100**		**100**		**100**		**100**	
Lac+ 0	93,2	0,2	86,8	0,7	76,2	0,9	52,7	1,5	28,1	0,7	19,2	1,0	92,3	0,6	86,8	0,6	80,3	1,5	59,0	2,7	30,8	1,4	18,9	0,4
Lac +1	2,8	0,1	2,7	0,0	2,3	0,0	1,6	0,0	0,9	0,0	0,7	0,0	2,8	0,0	2,7	0,1	2,4	0,1	1,8	0,1	1,0	0,0	0,7	0,0
Lac +2							1,2	0,0	1,9	0,0	2,2	0,1							1,0	0,1	1,8	0,0	2,3	0,1
Lac +3	4,0	0,3	10,4	0,7	21,4	0,9	44,5	1,5	69,1	0,7	78,0	1,0	4,8	0,5	10,5	0,7	17,3	1,5	38,1	2,8	66,3	1,4	78,2	0,5
Sum	**100**		**100**		**100**		**100**		**100**		**100**		**100**		**100**		**100**		**100**		**100**		**100**	
ALA +0	96,7	0,1	96,1	0,0	94,3	0,4	86,1	0,1	59,1	0,8	40,9	1,1	96,9	0,0	96,7	0,0	96,1	0,1	92,5	0,3	75,6	1,1	54,8	0,3
ALA +1	2,8	0,1	2,8	0,1	2,8	0,0	2,6	0,0	1,8	0,0	1,3	0,0	2,9	0,0	2,8	0,0	2,8	0,1	2,7	0,1	2,3	0,0	1,7	0,0
ALA +3	0,4	0,0	1,1	0,1	3,0	0,3	11,3	0,0	39,1	0,8	57,8	1,1	0,2	0,0	0,5	0,0	1,1	0,1	4,8	0,3	22,0	1,2	43,5	0,3
Sum	**100**		**100**		**100**		**100**		**100**		**100**		**100**		**100**		**100**		**100**		**100**		**100**	
GLN +0	94,6	0,0	94,6	0,0	94,6	0,0	94,6	0,0	94,6	0,0	94,6	0,0	94,6	0,0	94,6	0,0	94,6	0,0	94,6	0,0	94,6	0,0	94,6	0,0
GLN +1	5,4	0,0	5,4	0,0	5,4	0,0	5,4	0,0	5,4	0,0	5,4	0,0	5,4	0,0	5,4	0,0	5,4	0,0	5,4	0,0	5,4	0,0	5,4	0,0
Sum	**100**		**100**		**100**		**100**		**100**		**100**		**100**		**100**		**100**		**100**		**100**		**100**	
GLU +0	95,5	0,2	95,4	0,1	95,5	0,0	95,3	0,2	93,6	0,1	91,3	0,2	95,5	0,1	95,3	0,1	95,2	0,1	93,8	0,0	87,0	0,5	79,6	0,4
GLU +1	4,5	0,2	4,6	0,1	4,5	0,0	4,7	0,2	4,9	0,0	5,0	0,1	4,5	0,1	4,7	0,1	4,8	0,1	4,9	0,1	5,1	0,1	5,1	0,1
GLU +2									1,5	0,1	3,7	0,1							1,2	0,0	6,8	0,4	11,9	0,2
GLU +3																					0,7	0,1	1,7	0,1
GLU +4																					0,5	0,0	1,4	0,0
GLU +5																							0,2	0,1
Sum	**100**		**100**		**100**		**100**		**100**		**100**		**100**		**100**		**100**		**100**		**100**		**100**	